**Article ID**: 1000-7032(2015)02-0176-10

# Hydrothermal Synthesis and High Activity of $Bi_2S_3$/BiOCl Composite Photocatalysts

LI Hui-quan[1,2], ZHU Liang-jun[1,2], SUN Qian[1], WANG Gao[1], MIAO Hui[1,2], CUI Yu-min[1,2*], JIA Qing-feng[1]

(1. *College of Chemistry and Materials Engineering, Fuyang Normal College, Fuyang* 236037, *China*;
2. *Anhui Provincial Key Laboratory for Degradation and Monitoring of Pollution of The Environment, Fuyang* 236037, *China*)

* *Corresponding Author, E-mail: cuiyumin*0908@163.*com*

**Abstract**: $Bi_2S_3$/BiOCl composite photocatalysts with various mass fractions of $Bi_2S_3$ were successfully synthesized by a facile hydrothermal process at 433 K, characterized by various techniques, and evaluated by the photo-degradation of methyl orange (MO) in an aqueous solution under the irradiation of ultraviolet (UV) light. The results showed that the photocatalytic activity of $Bi_2S_3$/BiOCl catalysts was greatly enhanced, compared with that of pure $Bi_2S_3$ and BiOCl. Especially, the photocatalytic activity of the 26.5% $Bi_2S_3$/BiOCl sample is very close to that of commercial Degussa P-25 ($TiO_2$), which has been generally recognized as an efficient photocatalyst under UV light irradiation. The remarkably enhanced photocatalytic activity could be mainly attributed to the effective transfer of the photo-generated electrons and holes at the heterojunction interface of $Bi_2S_3$ and BiOCl, which reduced the recombination of electron-hole pairs.

**Key words**: hydrothermal method; $Bi_2S_3$/BiOCl; composite photocatalysts; methyl orange
**CLC number**: O634 **Document code**: A **DOI**: 10.3788/fgxb20153602.0176

# $Bi_2S_3$/BiOCl 复合光催化剂的水热合成及其高活性

李慧泉[1,2], 朱良俊[1,2], 孙 倩[1], 王 高[1], 苗 慧[1,2], 崔玉民[1,2*], 郑青峰[1]

(1. 阜阳师范学院 化学与材料工程学院, 安徽 阜阳 236037;
2. 安徽环境污染物降解与监测省级实验室, 安徽 阜阳 236037)

**摘要**: 采用一种简便的水热法在433 K的温度下成功合成了具有不同$Bi_2S_3$质量分数的$Bi_2S_3$/BiOCl复合光催化剂,利用各种技术对其进行了表征。在紫外光照射下,以甲基橙水溶液的光催化降解为模型反应,评价了$Bi_2S_3$/BiOCl复合光催化剂的活性。研究结果表明:与纯$Bi_2S_3$和纯BiOCl相比,$Bi_2S_3$/BiOCl样品明显具有更高的光催化性能,尤其当$Bi_2S_3$在$Bi_2S_3$/BiOCl中的质量分数为26.5%时,$Bi_2S_3$/BiOCl复合催化剂的光催化活性与商业P25($TiO_2$)的活性非常接近,而这种商业P25在紫外光照射下是公认的高效光催化剂。这种明显提高的光催化活性主要归功于光生电子和空穴在$Bi_2S_3$和BiOCl形成异质结界面上的有效转移,降低了电子-空穴对的复合。

**关 键 词**: 水热法; $Bi_2S_3$/BiOCl; 复合光催化剂; 甲基橙

**收稿日期**: 2014-11-03; **修订日期**: 2014-12-02
**基金项目**: 国家自然科学基金(21201037); 安徽省高校自然科学基金(kj2014a191); 安徽省自然科学基金(1408085mb35); 安徽省高校青年人才基金(2013sqrl058zd); 功能性分子固体省部共建教育部重点实验室项目(14010); 阜阳师范学院和安徽环境污染物降解与监测省级实验室项目(fsb201401003,2014kjfh01)资助

# 1 Introduction

The photocatalytic material has been an exciting and rapidly growing research area owing to its great potential applications in solar energy utilization, photocatalytic hydrogen evolution, organic wastewater treatment and air purification[1-8]. Bismuth oxychloride (BiOCl), as one of the best nanomaterials, has recently attracted intensive attention in the degradation of environmental pollutants due to its interesting chemical and physical properties[9-11], such as electrical and optical performances, band gaps, and special micro/nanostructures. However, the low quantum efficiency of photocatalytic reactions resulting from the high rate of electron-hole recombination, impair its applications to great extent. As a result, in order to overcome this disadvantage, many attempts have been done, including doping or composition tuning, controlling the morphologies, and forming heterojunctions or composite structures[12-14].

$Bi_2S_3$ has a narrow band-gap energy of ~1.3 eV[15], therefore, it may be a potential sensitizer to sensitize BiOCl with a wide band-gap energy (3.19 – 3.60 eV)[10]. In 2012, Kang *et al.*[16] reported that the production of hydrogen of $Bi_2S_3$-loaded $TiO_2$ ($Bi_2S_3/TiO_2$) was higher than that of pure $TiO_2$ and $Bi_2S_3$ under identical experiment conditions. The improved performance could be attributed to the fact that $Bi_2S_3$-loaded $TiO_2$ facilitated the separation of photo-generated carriers. Hence, $Bi_2S_3$/BiOCl composite may be an ideal system to enhance the separation efficiency of photo-generated charge carriers, and then achieve a high photocatalytic activity. Recent studies have also showed that $Bi_2S_3$-sensitized BiOCl photocatalyst[17], $Bi_2S_3$/BiOCl composites[18] and $Bi_2S_3$ nanocrystals/BiOCl hybrid architectures[19] synthesized by an ion exchange method had higher visible light photocatalytic activities than single $Bi_2S_3$ and BiOCl. However, to the best of our knowledge, the researches on the UV light photocatalytic activity and mechanism in the $Bi_2S_3$/BiOCl system prepared by a hydrothermal method have not been reported.

In this work, $Bi_2S_3$/BiOCl composite photocatalysts with different mass fraction of $Bi_2S_3$ were successfully synthesized by a facile hydrothermal process at 433 K, and the obtained samples were characterized by various techniques. As a representative of organic dyes released in the textile effluents, methyl orange (MO) was used to evaluate the photocatalytic activity of $Bi_2S_3$/BiOCl catalysts under UV light irradiation, and the photocatalytic mechanism of $Bi_2S_3$/BiOCl catalysts was discussed. The facile preparation of $Bi_2S_3$/BiOCl with high activity could be hopefully applied in the near future.

# 2 Experiments

## 2.1 Materials

All of the reagents were provided by Sinopharm Chemical Reagent Co., Ltd. (China) except that $TiO_2$ powder (Degussa P-25) was purchased from Degussa Co. (Frankfurt, Germany), and P25 was used as the reference. Bismuth nitrate pentahydrate [$Bi(NO_3)_3 \cdot 5H_2O$], thiourea ($CH_4N_2S$), sodium hydroxide (NaOH), absolute ethanol ($CH_3CH_2OH$), nitric acid ($HNO_3$), potassium chloride (KCl) and ethylene glycol ($OH\text{-}CH_2CH_2\text{-}OH$) were of analytical grade.

## 2.2 Catalyst Preparation

The $Bi_2S_3$/BiOCl catalysts were synthesized by a hydrothermal method. In a typical preparation, different stoichiometric amounts of $Bi(NO_3)_3 \cdot 5H_2O$ and 0.27 g thiourea were dissolved in 20 mL of 0.10 mol/L $HNO_3$ solution. The mixture was stirred and sonicated until the $Bi(NO_3)_3 \cdot 5H_2O$ was dissolved, and the pH value of mixed solution was adjusted to 7.0 with a certain concentration of NaOH solution, followed by the addition of 0.15 g KCl and 30 mL ethylene glycol solution. Then the mixture was transferred to a Teflon-lined stainless steel autoclave to perform hydrothermal process at 433 K for 24 h. After cooling down to room temperature, the obtained products were separated centrifugally, washed with absolute ethanol and de-ionized water and dried at 373 K in air. The final $Bi_2S_3$/BiOCl samples with various mass fractions of $Bi_2S_3$ of 0, 13.3%, 26.5% and 39.8%, respectively, were denoted as 0, 13.3%, 26.5% and 39.8% $Bi_2S_3$/

BiOCl, respectively. For comparison, pure $Bi_2S_3$ sample was also synthesized by adopting the same method at the absence of KCl and ethylene glycol.

### 2.3 Catalyst Characterization

X-ray diffraction (XRD) was performed on a Philips X'pert diffractometer equipped with Ni-filtered Cu Kα radiation source ($\lambda = 0.154\ 18$ nm). X-ray photoelectron spectroscopy (XPS) measurements were carried out by using Multilab 2000 XPS system with a monochromatic Mg Kα source and a charge neutralizer. All binding energies were calibrated using C 1s peak at 284.6 eV. The Brunauer-Emmett-Teller (BET) surface areas and pore volume of samples were determined from $N_2$ adsorption isotherms at 77 K using a Micromeritics ASAP 2020 instrument with a computer-controlled measurement system. High-resolution transmission electron microscopy (HR-TEM) images were taken using a JEM-2100 electron microscope. The photoluminescence (PL) spectra, obtained at room temperature with an excitation wavelength of 280 nm, were recorded on a CARY Eclipse (America) fluorescence spectrophotometer. UV-Vis diffuse reflection spectroscopy of the catalysts was determined with a Shimadzu UV-3600 spectrophotometer (Japan).

### 2.4 Photocatalytic Reaction

The photocatalytic activities of $Bi_2S_3$/BiOCl catalysts were evaluated by the degradation of MO in an aqueous solution. UV light was obtained by a 300 W high-pressure mercury lamp ($\lambda_{max} = 365$ nm). For each UV light test, 40 mL MO ($6.11 \times 10^{-5}$ mol/L) aqueous solution and 0.05 g catalyst sample were used. A general procedure was carried out as follows. First, MO aqueous solution was placed into a water-jacketed reactor maintained at 298 K, and then the catalyst samples were suspended in the solution. The suspension was stirred vigorously for 60 min in the dark to establish the adsorption-desorption equilibrium of MO, then irradiated under UV light. About 2.5 mL solution was withdrawn from the reactor periodically and centrifuged and analyzed for the degradation of MO using a TU-1901 spectrophotometer.

For the detection of •OH, catalyst samples (0.05 g) were dispersed in a 10 mL of terephthalic acid (TA) solution whose concentration was set at $5 \times 10^{-4}$ mol/L in $2 \times 10^{-3}$ mol/L NaOH solution. At a fixed time intervals, the suspension solution was sampled, centrifuged and measured on a Varian Cary Eclipse type fluorescence spectrophotometer. The excitation wavelength was 315 nm.

In order to study the effect of •OH, isopropanol (IPA) quencher (5.0 μL), as an •OH scavenger, was introduced into the photocatalytic degradation process of MO in a manner similar to the photo-degradation experiment.

## 3 Results and Discussion

### 3.1 Catalyst Structure

Fig. 1 shows the XRD patterns of $Bi_2S_3$/BiOCl samples with different $Bi_2S_3$ mass fraction. Five main diffraction peaks of $Bi_2S_3$ were found and could be respectively indexed to the (130), (211), (221), (431) and (351) planes of orthorhombic $Bi_2S_3$ (JCPDS card No. 17-0320). The characteristic diffraction peaks of BiOCl including (101), (110), (112), (200), (211) and (212) are in good accordance with the standard card of tetragonal BiOCl (JCPDS card No. 06-0249). For the $Bi_2S_3$/BiOCl samples, the intensities of corresponding diffraction peaks of $Bi_2S_3$ strengthened gradually along with the increase of the $Bi_2S_3$ contents in the $Bi_2S_3$/BiOCl composites, while those of BiOCl weakened simultaneously for its depletion. No other characteristic peaks of impurity were detected, indicating that $Bi_2S_3$/BiOCl composites are only composed of $Bi_2S_3$ and BiOCl phases at the same time.

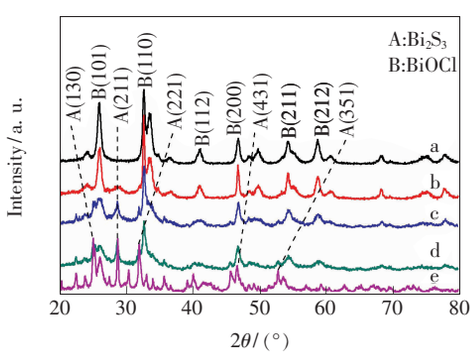


Fig. 1 XRD patterns of $Bi_2S_3$/BiOCl samples with different $Bi_2S_3$ mass fraction: (a) 0.00, (b) 13.3, (c) 26.5, (d) 39.8, (e) 100.

The average crystallite sizes of $Bi_2S_3$ and BiOCl in the $Bi_2S_3$/BiOCl samples were calculated by the Scherrer formula (Eq.(1))[20], respectively, as shown in Table 1.

$$L = K\lambda/(\beta\cos\theta), \quad (1)$$

Where $L$ is taken as average crystallite size, $K$ is a constant equalling to 0.89, $\lambda$ is 0.154 nm, $\beta$ is the full-width of half-maximum measured in radians on the $2\theta$ scale, $\theta$ is the Bragg angle for the diffraction peaks.

**Table 1　Average crystallite size ($L$), BET surface areas ($S_{BET}$), pore volumes ($V_{BJH}$) and photocatalytic activity of different catalyst (reaction for the first one hour)**

| Sample | $L$/nm | | $S_{BET}$/ ($m^2 \cdot g^{-1}$) | $V_{BJH}$ ($cm^3 \cdot g^{-1}$) | MO degradation/ % |
|---|---|---|---|---|---|
| | $Bi_2S_3$ | BiOCl | | | |
| $Bi_2S_3$ | 16.9 | — | 19.7 | 0.123 | 10.8 |
| 13.3% $Bi_2S_3$/BiOCl | 14.8 | 18.2 | 43.1 | 0.258 | 77.0 |
| 26.5% $Bi_2S_3$/BiOCl | 11.7 | 16.7 | 49.3 | 0.306 | 94.0 |
| 39.8% $Bi_2S_3$/BiOCl | 15.3 | 18.6 | 41.4 | 0.189 | 52.2 |
| BiOCl | — | 20.3 | 7.70 | 0.016 | 65.7 |

Fig. 2 presents the HR-TEM image of 26.5% $Bi_2S_3$/BiOCl sample, in which the interface of $Bi_2S_3$ and BiOCl can be observed. Moreover, clear fringe with an interval of 0.360 nm can be indexed to (130) lattice plane of orthorhombic $Bi_2S_3$ and that of 0.275 nm agreed with the (110) lattice plane of tetragonal BiOCl, which further demonstrates the existence of the heterojunction formed between $Bi_2S_3$ and BiOCl.

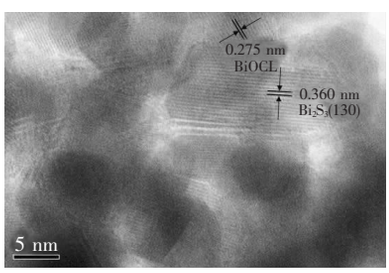


Fig. 2　HR-TEM image of 26.5% $Bi_2S_3$/BiOCl sample

The chemical state of as-prepared 26.5% $Bi_2S_3$/BiOCl sample was investigated by using X-ray photoelectron spectroscopy (XPS), and the results are shown in Fig. 3. The typical XPS survey spectrum in Fig. 3(a) shows that 26.5% $Bi_2S_3$/BiOCl was composed of Bi, Cl, S and O elements (C 1s peak can be ascribed to the adventitious hydrocarbon from XPS instrument itself). The Bi 4f peaks of the sample appeared at 164.5 and 159.2 eV in Fig. 3(b), and the Cl 2p peaks of the sample appeared at 198.0 and 199.4 eV in Fig. 3(c). The binding energies of both Bi 4f and Cl 2p were in agreement with the reported values in the literature[21]. In Fig. 3(d), the O 1s binding energy of 530.1 eV could be attributed to the lattice oxygen in crystalline BiOCl[22].

Fig. 4(a), (b) and (c) display the UV-Vis diffuse reflectances spectroscopy of $Bi_2S_3$, BiOCl and 26.5%$Bi_2S_3$/BiOCl samples. It can be seen that the absorption edge of BiOCl is located at about 378 nm, while $Bi_2S_3$ has strong absorption over the whole visible light region. As for 26.5% $Bi_2S_3$/BiOCl sample, its absorption edge (~370 nm) shifts to shorter wavelengths compared to that of BiOCl, which may be attributed to small particle sizes of 26.5% $Bi_2S_3$/BiOCl.

As a crystalline semiconductor, the optical absorption near the band edge follows the formula $\alpha h\nu = A(h\nu - E_g)^{n/2}$, where $\alpha$, $\nu$, $E_g$, and $A$ are the absorption coefficient, light frequency, band-gap energy, and a constant, respectively[23]. As reported previously, the $n$ values of $Bi_2S_3$[17] and BiOCl[24] are 1 and 4, respectively. The band-gap energies ($E_g$) of BiOCl and $Bi_2S_3$ can be thus estimated from a plot of $(\alpha h\nu)^{1/2}$ and $(\alpha h\nu)^2$ *vs.* photon energy ($h\nu$), respectively. As shown in Fig. 4(d), the intercept of the tangent to the $x$-axis will give a good approximation of the band-gap energies for the BiOCl and $Bi_2S_3$ powders, respectively. The estimated $E_g$ values are about 3.28 and 1.28 eV for pure BiOCl and $Bi_2S_3$, respectively, which are very close to the

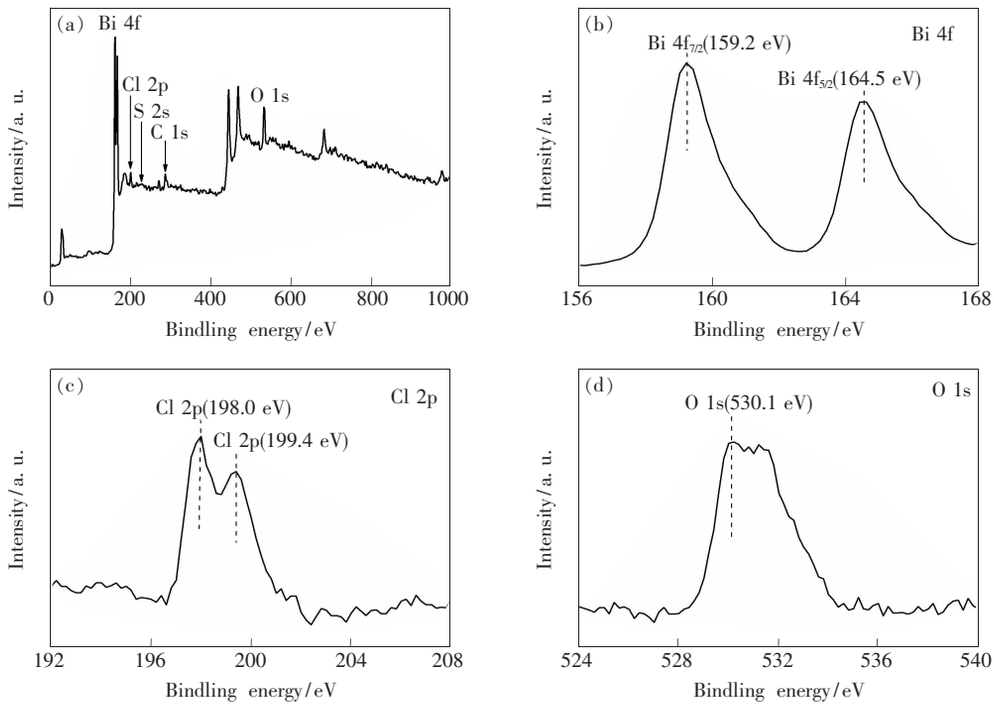


Fig. 3 XPS survey spectra of 26.5% $Bi_2S_3$/BiOCl (a) and the corresponding high-resolution XPS spectra of Bi 4f (b), Cl 2p (c) and O 1s (d).

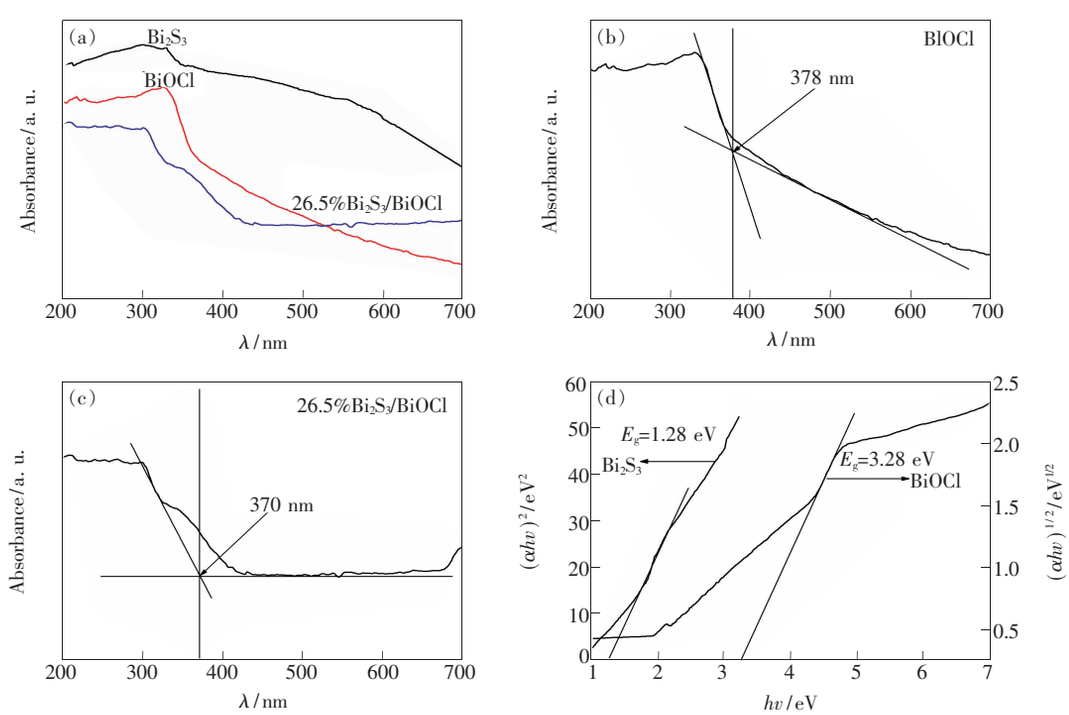


Fig. 4 UV-Vis diffuse reflectance spectra of $Bi_2S_3$, BiOCl and 26.5% $Bi_2S_3$/BiOCl samples (a – c), and plot of $(\alpha h\nu)^{2/n}$ *vs.* energy ($h\nu$) for the band-gap energy of $Bi_2S_3$ and BiOCl (d).

values reported in the literatures[10,25].

The data related to BET surface areas and pore volumes obtained from $N_2$ adsorption-desorption analysis are also summarized in Table 1. It can be seen that with $Bi_2S_3$ content increasing, the BET surface areas and pore volumes of $Bi_2S_3$/BiOCl catalysts first increase, reaching the maximums at $Bi_2S_3$ mass fraction of 26.5%, respectively, and then

decrease with further increasing $Bi_2S_3$ contents. The BET surface areas and pore volumes of $Bi_2S_3$/BiOCl catalysts are obviously higher than those of pure $Bi_2S_3$ and BiOCl, but the corresponding BET surface areas of 13.3%, 26.5% and 39.8% $Bi_2S_3$/BiOCl catalysts did not have obvious difference, which demonstrates that the BET surface area is not the main influencing factor for the photocatalytic activity of different $Bi_2S_3$/BiOCl catalysts.

### 3.2 Photocatalytic Activity

The effect of $Bi_2S_3$ mass fraction on the photocatalytic activity of $Bi_2S_3$/BiOCl catalysts has been investigated by MO degradation in an aqueous solution under UV light irradiation. Fig. 5(a) shows the UV light photocatalytic activity of $Bi_2S_3$/BiOCl catalysts with different $Bi_2S_3$ content. It can be seen that the self-degradation of MO is very low under UV light irradiation, indicating that the photolysis can be ignored. While $Bi_2S_3$, BiOCl and $Bi_2S_3$/BiOCl catalysts exhibit obviously the photo-degradation of MO, and $Bi_2S_3$ content in BiOCl exerts great influences on the photocatalytic activity of $Bi_2S_3$/BiOCl catalysts. With the increasing of $Bi_2S_3$ mass fraction, the photocatalytic activity of $Bi_2S_3$/BiOCl catalysts first increases, reaching a maximum at $Bi_2S_3$ mass fraction of 26.5%, then decreases, and under 60 min UV light irradiation, the maximum MO degradation ratio reaches to 94.0%, being very close to that of commercial Degussa P-25, which has been generally recognized as an efficient photocatalyst under UV light irradiation.

In generally, the photocatalytic activity of composite catalyst is related to its BET surface areas, component contents, band structure matching and heterojunction interface, *etc.* But the corresponding BET surface areas (Table 1) of 13.3%, 26.5%, 39.8% $Bi_2S_3$/BiOCl catalysts do not have obvious difference, which demonstrates that the main influencing factor for the enhanced photocatalytic performance of $Bi_2S_3$/BiOCl catalysts is more likely to be the heterojunction structure rather than both BET surface areas. With the increasing of $Bi_2S_3$ mass fraction from 13.3% to 26.5%, the more $Bi_2S_3$-BiOCl heterojunction interface will be formed, which facilitates

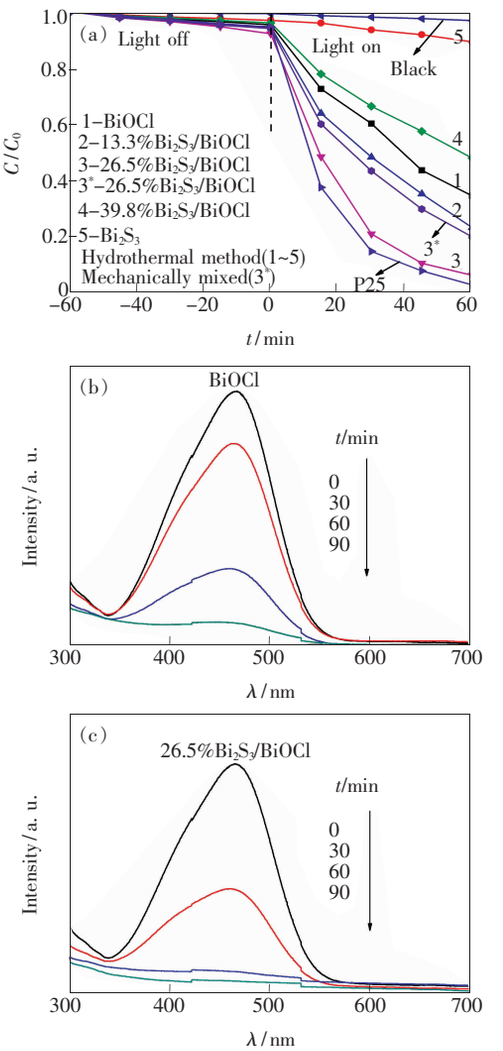


Fig. 5　Effects of $Bi_2S_3$ mass fraction in the $Bi_2S_3$/BiOCl catalysts on the degradation of MO under UV light irradiation (a), and UV-Vis spectra of the MO aqueous solution under UV light irradiation in the presence of BiOCl (b) and 26.5% $Bi_2S_3$/BiOCl (c) catalysts.

the efficient separation of photo-induced electrons and holes, leading to the enhanced photocatalytic performance. However, if the mass fraction of $Bi_2S_3$ increases continuously to excess, more $Bi_2S_3$ and $Bi_2S_3$ contacts will be established, which dominates the $Bi_2S_3$ and BiOCl contacts. The $Bi_2S_3$ and $Bi_2S_3$ contacts are not as effective as $Bi_2S_3$ and BiOCl contacts for an effective charge separation. Moreover, the excessive $Bi_2S_3$ with narrow band gap can act as the recombination center of electrons and holes, impeding the photocatalytic activity on the contrary[15-16,21,25]. Thus, 26.5% $Bi_2S_3$/BiOCl exhibits the highest photocatalytic activity.

In order to confirm the advantage of heterojunction between $Bi_2S_3$ and BiOCl, 26.5% $Bi_2S_3$/BiOCl is compared with the mechanical mixture of $Bi_2S_3$ and BiOCl with the similar composition under identical photocatalytic degradation conditions, as shown in Fig. 5(a). Obviously, the UV light photocatalytic activity of mechanically mixed 26.5% $Bi_2S_3$/BiOCl are lower than that of 26.5% $Bi_2S_3$/BiOCl prepared by hydrothermal method. This is mainly because $Bi_2S_3$ and BiOCl behave as independent photocatalysts rather than a coupled system in the mechanical mixture of $Bi_2S_3$ and BiOCl, which is unfavorable to the transfer of charge carriers from one phase to another. However, the photocatalytic activity of mechanical mixture of $Bi_2S_3$ and BiOCl is enhanced compared with that of pure $Bi_2S_3$ and BiOCl, even the mathematical sum of them. This might be owing to the inevitable partial contact between $Bi_2S_3$ and BiOCl in the mechanical mixture of $Bi_2S_3$ and BiOCl, which is in favor of the photocatalytic activity to some extent but is still far inferior to the effect of $Bi_2S_3$/BiOCl heterostructure[25]. The results show that the $Bi_2S_3$ and BiOCl heterojunction fabricated in the $Bi_2S_3$/BiOCl catalysts can improve the photocatalytic activity greatly.

UV-Vis spectra of MO aqueous solution as a function of UV light irradiation time in the presence of pure BiOCl and 26.5% $Bi_2S_3$/BiOCl catalysts are illustrated in Fig. 5(b) and Fig. 5(c), respectively. It can be seen that the visible region peak intensities in the photo-degradation of MO by the 26.5% $Bi_2S_3$/BiOCl catalyst decrease more obviously than those of pure BiOCl catalyst after 60 min UV light irradiation, which is in agreement with the results of Fig. 5(a). Since no new peak appears, the loss of absorbance can be mainly attributed to the degradation reaction.

### 3.3 Discussion of The Photocatalytic Mechanism

#### 3.3.1 Hydroxyl Radical (•OH) Involved in The Photocatalytic Process

Hydroxyl radical (•OH) has been considered to be an important species in the photocatalytic degradation of many hazardous chemical compounds owing to its high reaction ability to attack organic molecule. The formation of •OH on the surface of $Bi_2S_3$, BiOCl and 26.5% $Bi_2S_3$/BiOCl catalysts was detected by a photoluminescence (PL) technique with terephthalic acid as a probe molecule. Terephthalic acid reacted with •OH readily to produce a highly fluorescent product, 2-hydroxy terephthalic acid, whose PL peak intensity was in proportion to the amount of •OH radicals produced in water, which was reported in the literature [26]. After UV light irradiation for a fixed time, the reaction solution was filtrated to measure the PL intensity at 425 nm of 2-hydroxyterephthalic acid.

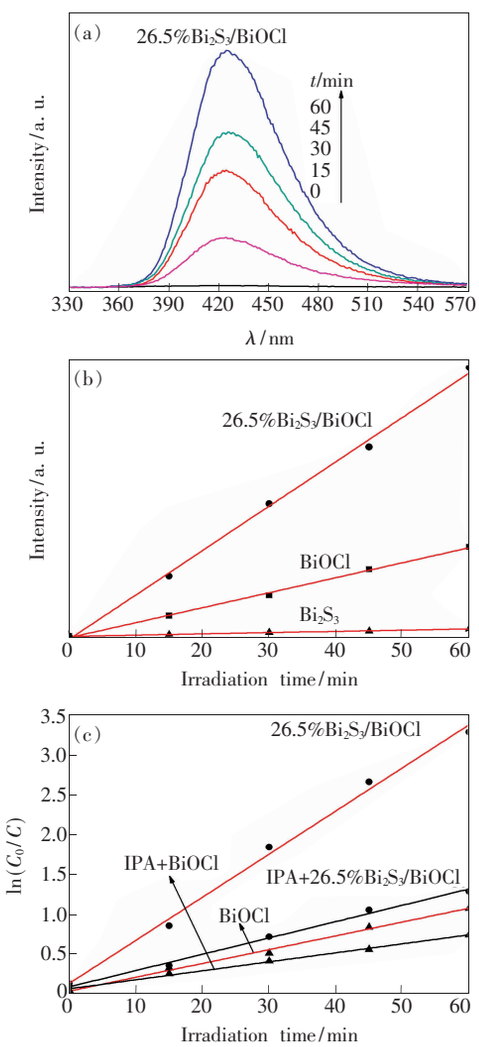


Fig. 6 Changes of PL spectra over 26.5% $Bi_2S_3$/BiOCl (a), linear transform of PL spectra over different catalyst recorded during UV light illumination in terephthalic acid solution ($5 \times 10^{-4}$ mol/L, excitation at 315 nm) (b), and the kinetics of photocatalytic degradation of MO using different catalyst under UV light illumination (c).

Fig. 6(a) indicates the changes of PL spectra of 26.5% $Bi_2S_3$/BiOCl catalyst in a $5 \times 10^{-4}$ mol/L terephthalic acid solution with UV irradiation time. It can be seen that no PL signal is observed in the absence of irradiation. The fluorescence intensity at 425 nm gradually increase with the irradiation time, which elucidates that •OH on 26.5% $Bi_2S_3$/BiOCl have been really produced under UV light irradiation.

As shown in Fig. 6(b), the PL peak of 26.5% $Bi_2S_3$/BiOCl is higher than that of pure BiOCl and $Bi_2S_3$ under UV light irradiation, and it suggests that the formation rate of OH radicals on its surface is much higher than that of pure BiOCl and $Bi_2S_3$, which implies the photocatalytic activity of the 26.5% $Bi_2S_3$/BiOCl catalyst is much higher than that of pure BiOCl and $Bi_2S_3$. This result is also verified in the Fig. 5(a).

In order to identify the role of •OH in the MO degradation, IPA, an efficient •OH quencher[27] was added into BiOCl and 26.5% $Bi_2S_3$/BiOCl reaction systems. The results are shown in Fig. 6(c). It can be seen that the degradation efficiency ($k_{app}$) of MO decreases significantly after the addition of IPA under UV light irradiation. That is to say, the •OH species plays an important role in the degradation of MO under UV light irradiation.

### 3.3.2　Origin of •OH

Taking the kinds of •OH species involved in the photocatalysis into account, the photocatalytic process of $Bi_2S_3$/BiOCl catalysts can be described as the following Eqs. (2) - (6):

$$Bi_2S_3/BiOCl + h\nu \rightarrow e^- + h^+, \quad (2)$$

$$3e^- + O_2 + 2H^+ \rightarrow \cdot OH + OH^-, \quad (3)$$

$$H_2O + h^+ \rightarrow \cdot OH + H^+, \quad (4)$$

$$OH^- + h^+ \rightarrow \cdot OH, \quad (5)$$

$$MO + \cdot OH \rightarrow \text{products}. \quad (6)$$

In the above process, electron-hole pairs are directly produced by catalyst after UV light illumination. Then, the photo-generated electrons transfer to CB bottom of the catalyst and react with the adsorbed $O_2$ and $H^+$ on the surface of catalyst to form •OH. Meanwhile, the holes are left on the VB top, reacting with the adsorbed $H_2O$ or $OH^-$ on the surface of catalyst to form •OH. After that, the •OH species oxidized MO.

### 3.3.3　Mechanism of Photocatalytic Activity Enhancement of $Bi_2S_3$/BiOCl

It is well known that the energy level and the band gap of semiconductors play important roles in determining their photocatalytic activities. Using two semiconductors in contact with different redox energy levels of conduction band (CB) and valence band (VB) can be used to improve photo-generated carriers separation and enhance the efficiency of the interfacial charge transfer[28]. In the light of the experiment results and by referring to the literatures[13-17,25], the transfer behaviors of the photo-generated electrons and holes in $Bi_2S_3$/BiOCl catalysts are illustrated in Fig. 7. As shown, the CB and VB of $Bi_2S_3$ lie above those of BiOCl. Clearly, the difference between energy bands of BiOCl and $Bi_2S_3$ (Fig. 7) allows the efficient transfer of electron and hole between them. When the $Bi_2S_3$/BiOCl catalyst is irradiated by UV light, BiOCl and $Bi_2S_3$ are both excited; then, a large number of electrons and holes are produced in the system. Electrons will transfer from $Bi_2S_3$ to CB of BiOCl and holes shift from BiOCl to VB of $Bi_2S_3$ at the same time. In this way, the photo-generated electron-hole pairs are effectively separated, and the better separation of electrons and holes in the $Bi_2S_3$/BiOCl catalysts can be confirmed by photoluminescence (PL) emission spectra in Fig. 8.

PL emission spectra have been widely used to investigate the separation efficiency of the photo-generated charge carriers in a semiconductor[29]. The comparison of PL spectra (excited by 280 nm) of pure BiOCl and 26.5% $Bi_2S_3$/BiOCl at room temperature

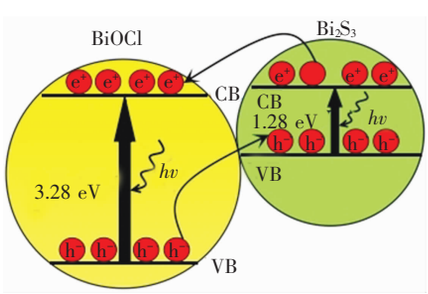


Fig. 7　Diagrams of photo-generated electron-hole pairs transfer of $Bi_2S_3$ and BiOCl

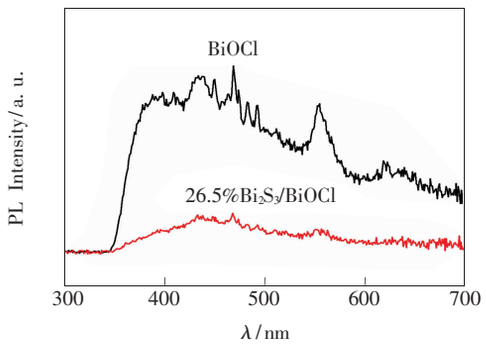


Fig. 8 Photoluminescence (PL) spectra of pure $Bi_2S_3$ and 26.5% $Bi_2S_3$/BiOCl samples recorded at room temperature with the excitation wavelength of 280 nm

is shown in Fig. 8. It can be seen that the two catalysts have a broad emission peak, and the strongest emitting peaks are similar, while PL emission intensity of the 26.5% $Bi_2S_3$/BiOCl sample isdramatically weakened compared with that of pure BiOCl, indicating that the recombination of photo-generated charge carriers is greatly inhibited by the $Bi_2S_3$ introduction. In other words, a proper content of $Bi_2S_3$ in the BiOCl is helpful to separate the photo-generated charge carriers and increase the lifetime of charge carriers, and then enhance the photocatalytic activity of $Bi_2S_3$/BiOCl catalysts.

## 4 Conclusion

In summary, we have successfully synthesized the $Bi_2S_3$/BiOCl composite photocatalysts with different $Bi_2S_3$ mas fraction by a facile hydrothermal process at 433 K. The photocatalytic activity of $Bi_2S_3$/BiOCl catalyst is greatly enhanced, compared with that of pure $Bi_2S_3$ and BiOCl. Especially, the UV light photocatalytic activity of 26.5% $Bi_2S_3$/BiOCl catalyst is very close to that of commercial Degussa P-25. The remarkably enhanced photocatalytic performance can be mainly attributed to the effective transfer of the photo-generated electrons and holes at the heterojunction interface of $Bi_2S_3$ and BiOCl, which can reduce the recombination of electron-hole pairs. In this study, the simple and low-cost preparation route can not only reduce the energy consumption for the fabrication of $Bi_2S_3$/BiOCl catalysts but also might extend the utilization of $Bi_2S_3$/BiOCl at low temperature in the near future.

**References:**

[1] Chen X B, Liu L, Yu P Y, *et al*. Increasing solar absorption for photocatalysis with blank hydrogenated titanium dioxide nanocrystals [J]. *Science*, 2011, 331:746-750.

[2] Schwinghammer K, Mesch M B, Duppel V, *et al*. Crystalline carbon nitride nanosheets for improved visible-light hydrogen evolution [J]. *J. Am. Chem. Soc.*, 2014, 136(5):1730-1733.

[3] Li H Q, Hong W S, Cui Y M, *et al*. Enhancement of the visible light photocatalytic activity of $Cu_2O/BiVO_4$ catalysts synthesized by ultrasonic dispersion method at room temperature [J]. *Mater. Sci. Eng.* B, 2014, 181:1-8.

[4] Oncescu T, Stefan M I, Oancea P. Photocatalytic degradation of dichlorvos in aqueous $TiO_2$ suspensions [J]. *Environment. Sci. Technol.*, 2010, 17(3):1158-1166.

[5] Li H Q, Cui Y M, Hong W S, *et al*. Photodegradation of methyl orange by BiOI-sensitized $TiO_2$[J]. *Rare Metals* (稀有金属), 2012, 31(6):604-610 (in English).

[6] Chen S F, Hu Y F, Meng S G, *et al*. Study on the separation mechanisms of photogenerated electrons and holes for composite photocatalysts g-$C_3N_4$-$WO_3$[J]. *Appl. Catal.* B: *Environ.*, 2014, 150-151:564-573.

[7] Chen S F, Zhang S J, Liu W, *et al*. Preparation and activity evaluation of p-n junction photocatalyst NiO/$TiO_2$[J]. *J. Hazard. Mater.*, 2008, 155(1-2):320-326.

[8] Li H Q, Hong W S, Cui Y M, *et al*. High photocatalytic activity of C-$ZnSn(OH)_6$ catalysts prepared by hydrothermal method [J]. *J. Mol. Catal.* A: *Chem.*, 2013, 378:164-173.

[9] Shenawi-Khalil S, Uvarov V, Menes E, *et al*. New efficient visible light photocatalyst based on heterojunction of BiOCl-bismuth oxyhydrate [J]. *Appl. Catal.* A: *General*, 2012, 413-414:1-9.

[10] Mu Q H, Zhang Q H, Wang H Z, *et al*. Facile growth of vertically aligned BiOCl nanosheet arrays on conductive glass substrate with high photocatalytic properties [J]. *J. Mater. Chem.*, 2012, 22(33):16851-16857.

[11] Ye L Q, Deng K J, Xu F, *et al*. Increasing visible-light absorption for photocatalysis with black BiOCl [J]. *Phys. Chem.*

*Chem. Phys.*, 2012, 14(1):82-85.

[12] Li T B, Chen G, Zhou C, *et al.* New photocatalyst BiOCl/BiOI composites with highly enhanced visible light photocatalytic performances [J]. *Dalton Trans.*, 2011, 40(25):6751-6758.

[13] Xiong W, Zhao Q D, Li X Y, *et al.* One-step synthesis of flower-like Ag/AgCl/BiOCl composite with enhanced visible-light photocatalytic activity [J]. *Catal. Commun.*, 2011, 16(1):229-233.

[14] Shamaila S, Sajjad A K L, Chen F, *et al.* $WO_3$/BiOCl, a novel heterojunction as visible light photocatalyst [J]. *J. Colloid Interf. Sci.*, 2011, 356(2):465-472.

[15] Bessekhouad Y, Robert D, Weber J V. $Bi_2S_3$/$TiO_2$ and CdS/$TiO_2$ heterojunctions as an available configuration for photocatalytic degradation of organic pollutant [J]. *J. Photochem. Photobio.* A: *Chem.*, 2004, 163(3):569-580.

[16] Kim J, Kang M. Photocatalytic hydrogen production over the band gap-tuned urchin-like $Bi_2S_3$-loaded $TiO_2$composites system [J]. *Int. J. Hydrogen Energy*, 2012, 37:8249-8256.

[17] Cao J, Xu B Y, Lin H L, *et al.* Novel $Bi_2S_3$-sensitized BiOCl with highly visible light photocatalytic activity for the removal of rhodamine B [J]. *Catal. Commun.*, 2012, 26:204-208.

[18] Jiang S H, Zhou K Q, Shi Y Q, *et al.* Laser-assisted implantation of gold nanoparticles, formed under surface plasmon-polariton resonant conditions in polymer layer [J]. *Appl. Surf. Sci.*, 2014, 290:313-319.

[19] Cheng H F, Huang B B, Qin X Y, *et al.* A controlled anion exchange strategy to synthesize $Bi_2S_3$ nanocrystals/BiOCl hybrid architectures with efficient visible light photoactivity [J]. *Chem. Commun.*, 2012, 48(1):97-99.

[20] Sarwan B, Pare B, Acharya A D, *et al.* Mineralization and toxicity reduction of textile dye neutral red in aqueous phase using BiOCl photocatalysis [J]. *J. Photochem. Photobio.* B: *Bio.*, 2012, 116:48-55.

[21] Li H Q, Hong W S, Cui Y M, *et al.* Effect of $Mo_2C$ content on the structure and photocatalytic property of $Mo_2C$/$TiO_2$ catalysts [J]. *J. Alloys Compd.*, 2013, 569:45-51.

[22] Zhang X, Ai Z H, Jia F L, *et al.* Generalized one-pot synthesis, characterization, and photocatalytic activity of hierarchical BiO*X* (*X* = Cl, Br, I) nanoplate microspheres [J]. *J. Phys. Chem.* C, 2008, 112(3):747-753.

[23] Cao J, Xu B Y, Lin H L, *et al.* Novel heterostructured $Bi_2S_3$/BiOI photocatalyst: Acile preparation, characterization and visible light photocatalytic performance [J]. *Dalton Trans.*, 2012, 41(37):11482-11490.

[24] Pare B, Sarwan B, Jonnalagadda S B. Photocatalytic mineralization study of malachite green on the surface of Mn-doped BiOCl activated by visible light under ambient condition [J]. *Appl. Surf. Sci.*, 2011, 258(1):247-253.

[25] Yang L X, Sun W S, Luo S L, *et al.* White fungus-like mesoporous $Bi_2S_3$ ball/$TiO_2$ heterojunction with high photocatalytic efficiency in purifying 2,4-dichlorophenoxyacetic acid/Cr(Ⅵ) contaminated water [J]. *Appl. Catal.* B: *Environ.*, 2014, 156-157:25-34.

[26] Chen S F, Yang Y G, Liu W. Preparation, characterization and activity evaluation of TiN/F-$TiO_2$ photocatalyst [J]. *J. Hazard. Mater.*, 2011, 186(2-3):1560-1567.

[27] Cao J, Xu B Y, Lin H L, *et al.* Chemical etching preparation of BiOI/BiOBr heterostructures with enhanced photocatalytic properties for organic dye removal [J]. *Chem. Eng. J.*, 2012, 185-186:91-99.

[28] Zhao D, Chen C C, Yu C L, *et al.* Photoinduced electron storage in $WO_3$/$TiO_2$ nanohybrid material in the presence of oxygen and postirradiated reduction of heavy metal ions [J]. *J. Phys. Chem.* C, 2009, 113(30):13160-13165.

[29] Li H Q, Cui Y M, Hong W S. High photocatalytic performance of BiOI/$Bi_2WO_6$ toward toluene and reactive brilliant red [J]. *Appl. Surf. Sci.*, 2013, 264:581-588.

**李慧泉**（1973－），男，江西萍乡人，博士，教授，2012 年于南京大学获得博士学位，主要从事光催化纳米材料的设计与制备、结构与性能调控、光解水和水溶液中有机污染物的光催化降解等方面的研究。
E-mail: huiquanli0908@163.com

**崔玉民**（1963－），男，安徽亳州人，教授，1990 年于延边大学获得硕士学位，主要从事光催化方面的研究。
E-mail: cuiyumin0908@163.com